CrossMark

REVIEW

This section of Journal of Materials Research is reserved for papers that are reviews of literature in a given area.

Computational modeling of high-entropy alloys: Structures, thermodynamics and elasticity

Michael C. Gao[a)]
National Energy Technology Laboratory, Albany, Oregon 97321, USA; and AECOM, Albany, Oregon 97321, USA

Pan Gao
Department of Electrical and Computer Engineering, Tennessee State University, Nashville, Tennessee 37209, USA

Jeffrey A. Hawk
National Energy Technology Laboratory, Albany, Oregon 97321, USA

Lizhi Ouyang
Department of Physics and Astronomy, Tennessee State University, Nashville, Tennessee 37209, USA

David E. Alman
National Energy Technology Laboratory, Albany, Oregon 97321, USA

Mike Widom
Department of Physics, Carnegie Mellon University, Pittsburgh, Pennsylvania, USA

(Received 22 May 2017; accepted 15 August 2017)

This article provides a short review on computational modeling on the formation, thermodynamics, and elasticity of single-phase high-entropy alloys (HEAs). Hundreds of predicted single-phase HEAs were re-examined using various empirical thermo-physical parameters. Potential BCC HEAs (CrMoNbTaTiVW, CrMoNbReTaTiVW, and CrFeMoNbReRuTaVW) were suggested based on CALPHAD modeling. The calculated vibrational entropies of mixing are positive for FCC CoCrFeNi, negative for BCC MoNbTaW, and near-zero for HCP CoOsReRu. The total entropies of mixing were observed to trend in descending order: CoCrFeNi > CoOsReRu > MoNbTaW. Calculated lattice parameters agree extremely well with averaged values estimated from the rule of mixtures (ROM) if the same crystal structure is used for the elements and the alloy. The deviation in the calculated elastic properties from ROM for select alloys is small but is susceptible to the choice used for the structures of pure components.

I. INTRODUCTION

Since Yeh[1] and Cantor[2] independently reported their research on high-entropy alloys (HEAs) or equimolar multicomponent alloys in 2004, HEAs have attracted considerable interest from the scientific community, both in terms of developing a fundamental scientific understanding and potential technological applications.[3–5] However, to date, a variety of important questions still remain: In particular, what factors govern the formation of single-phase solid solution HEAs? What are the total number of possible single-phase equimolar HEA alloys with the face-centered cubic (FCC), body-centered cubic (BCC), and hexagonal close-packed (HCP) structures, respectively? For each crystal structure type, what is the maximum number of components that a single-phase HEA can possibly dissolve at high temperatures? How can the thermodynamic properties of single-phase HEAs be accurately predicted, given the assumed disordered atomic structures? What other entropy sources are possible, given the fact that the definition of HEAs by Yeh is based on the ideal configurational entropy? How can the elastic properties of single-phase HEAs be reliably calculated and how do they compare with their pure components?

Empirical thermo-physical parameters,[6–18] CALPHAD modeling,[19–29] phase diagram inspection,[25,30] ab initio molecular dynamics simulations,[3,25,30,31] hybrid Monte Carlo/molecular dynamic simulations (MC/MD),[32,33] and first-principles density functional theory (DFT) calculations[3,30,33–37] have all been used to predict the formation of single-phase HEAs. Gao[30] first evaluated the strengths and weaknesses among these methodologies, and concluded that rationally combining these techniques will likely speed up identification of new single-phase HEA compositions. It was also suggested at the time that hundreds of quaternary and higher-order equimolar

Contributing Editor: Susan B. Sinnott
[a)]Address all correspondence to this author.
e-mail: michael.gao@netl.doe.gov
DOI: 10.1557/jmr.2017.366

 © Materials Research Society 2017

https://doi.org/10.1557/jmr.2017.366 Published online by Cambridge University Press

compositions in the Dy–Er–Gd–Ho–Lu–Sc–Sm–Tb–Tm–Y, Ba–Ca–Eu–Sr–Yb, and Mo–Nb–Re–Ta–Ti–V–W systems may exist.[30] This work continues that investigation of those new single-phase HEAs that were mainly predicted by Bei,[38] Troparevsky,[14] Senkov,[39] and Gao[30] and also reports the possible existence of new potential septenary, octonary, and ennead BCC refractory HEAs. The thermodynamic mixing properties of FCC CoCrFeNi, BCC MoNbTaW, and HCP CoOsReRu are reviewed using CALPHAD, DFT, and MC/MD methods. The calculated elastic properties of single-phase HEAs with the FCC and BCC structures based on DFT calculations are then compared with the average values estimated from the rule of mixtures (ROM).

II. COMPUTATIONAL METHODOLOGIES AND DETAILS

A. DFT total energy calculations

The DFT calculations at zero temperature were performed using the VASP (Vienna Ab Initio Simulation Package, Vienna, Austria),[40,41] a plane-wave pseudo-potential software package. Projector augmented-wave potentials[42] were used as supplied with VASP and the Perdew–Burke–Ernzerhof[43] gradient approximation for the exchange-correlation functional. The semi-core 3*p*/4*p*/5*p* electrons of Cr, Fe, Mn, Mo, Nb, Ni, Os, Re, Ru, Ta, and W are explicitly treated as valence. The special quasi-random structure (SQS) method[44,45] was used to mimic the disordered atomic structures for equimolar HEAs as previously reported by Gao et al.[36] The cell size of the SQS models used in this work is: 64 atoms for quaternary HEAs, and 125, 125, and 160 atoms for quinary FCC, BCC, and HCP HEAs, respectively. For alloys that contain magnetic elements Co, Cr, Fe, Mn or Ni, collinear spin polarization (i.e., using ferromagnetic and anti-ferromagnetic spin configurations as initial input) were considered. The Brillouin-zone integrations were performed, using the Monkhorst–Pack *k*-point meshes.[46] The energy convergence with respect to *k*-points mesh is about 1–2 meV/atom. The plane-wave energy cutoff was held constant at 500 eV, 264 eV, and 322 eV for CoCrFeNi, MoNbTaW, and CoOsReRu, respectively. All SQS models first underwent a volumetric relaxation only (i.e., fixing the lattice shape and ionic positions), followed by full relaxation under zero pressure until the energy convergence reached 1 meV/atom. For simplicity, the zero-point energy was neglected in this study. The enthalpy of formation was calculated by subtracting the composition–weighted total energies of the constituent elements in their ground state from the total energy of the alloy.

Lattice phonon calculations were done using the harmonic approximation. The vibrational entropy (S^{vib}) is calculated by:

$$S^{\mathrm{vib}}(V,T) = 3k_{\mathrm{B}} \int_0^{\infty} n^{\mathrm{vib}} \times [(f_{\mathrm{BE}}+1)\ln(f_{\mathrm{BE}}+1) - f_{\mathrm{BE}}\ln f_{\mathrm{BE}}]\mathrm{d}\varepsilon \quad , \qquad (1)$$

where n^{vib} is the phonon DOS and f_{BE} is the Bose–Einstein distribution function.

Electronic excitation across the Fermi level by migrating electrons from the valance band to the conduction band gives rise to electronic entropy (S^{elec}), which can be determined by:

$$S^{\mathrm{elec}}(V,T) = -2k_{\mathrm{B}} \int_{-\infty}^{\infty} n^{\mathrm{elec}} \times [f_{\mathrm{FD}}\ln f_{\mathrm{FD}} + (1-f_{\mathrm{FD}})\ln(1-f_{\mathrm{FD}})]\mathrm{d}\varepsilon \quad , \qquad (2)$$

where n^{elec} is the electron DOS and f_{FD} is Fermi–Dirac distribution function.

B. MC/MD hybrid simulations

The hybrid MC/MD method proposed by Widom et al.[32,33] was used to calculate the configurational entropy. Supercells of 108, 128, and 96 atoms were used for FCC CoCrFeNi, BCC MoNbTaW, and HCP CoOsReRu, respectively. The simulations were done by alternating the molecular dynamics at each temperature with MC swaps, each performed from first principles using VASP. The canonical ensemble (i.e., constant amount of substance, volume, and temperature) was adopted for the FCC and BCC structures and the isothermal-isobaric ensemble (i.e., constant amount of substance, pressure and temperature) for the HCP structure. A minimum of 1000 MC steps with MD time steps of 10 or 20 fs were carried out for these three alloys, resulting in a total MD simulation time of greater than 10 ps. More details on the procedures used are provided elsewhere.[32,33,47,48] The reduction in configurational entropy due to a short-range chemical order can be calculated using the pairwise truncation of the Kikuchi cluster variation method[49]:

$$I = \sum_{i,j=1}^{N} y_{ij}\ln\left(y_{ij}/c_i c_j\right) \quad , \qquad (3)$$

where y_{ij} is the near neighbor correlations and c_i and c_j are the mole fractions of elements i and j, respectively.

C. CALPHAD modeling

The CALPHAD calculations were carried out using a TCNI8 thermodynamic database supplied by Thermo-Calc™ (Solna, Sweden).[50] For equilibrium calculations, all phases are restored. To calculate the entropy of mixing of the FCC and BCC phases, the ordered $L1_2$ and B2 phases were rejected. The TCNI8 database covers the

https://doi.org/10.1557/jmr.2017.366 Published online by Cambridge University Press

complete constituent binaries and limited ternaries.[50] Recent research[24–28] details the database development and applications of the CALPHAD modeling for HEAs.

III. STRUCTURES AND FORMATION

A. Re-examining those predicted single-phase compositions[14,30,38,39]

The new single-phase HEAs that were collected in Ref. 30 were mainly predicted by Bei,[38] Troparevsky,[14] Senkov,[39] and Gao.[30] Note that Troparevsky[14] did not specify the crystal structures of their predicted single-phase HEAs. The thermodynamic properties of most of these compositions are unknown and whether they would truly form a single-phase solid solution in the as-cast condition awaits experimental verification. To begin, those reassessed empirical rules[48] will be applied to these alloys.

The equations to calculate the empirical parameters are provided in the section of the Supplementary Material. The widely used parameters include the ideal configurational entropy $\left(S_{\text{ideal}}^{\text{conf}}\right)$, enthalpy of mixing in the liquid phase $\left(\Delta H_{\text{mix}}^{\text{liq}}\right)$,[6] atomic size difference (δ),[6] the Ω-parameter,[7] average valence electron concentration $\left(\overline{\text{VEC}}\right)$,[8] electronegativity difference ($\Delta\chi$),[9] the ϕ-parameter,[10] elastic residual strain root mean square ($\varepsilon_{\text{R.M.S.}}$, or $\sqrt{\langle\varepsilon^2\rangle}$),[11] the atomic size-related α_2-parameter,[12] intrinsic elastic strain energy (E_2/E_0),[12] the Φ-parameter,[13] the η-parameter,[14,48] and the κ_1^{cr} parameter.[15]

Very recently Gao et al.[48] assessed the most-up-to-date reported HEAs (single-phase, multiphase, and amorphous) and re-evaluated the effectiveness of those empirical rules. In general, the rules are useful since they are able to separate single-phase compositions from all amorphous compositions and many multiphase compositions. However, the threshold values are sensitive to the experimental data assessed, the atomic radii used, and whether or not two FCC or two BCC phases are counted as single-phase HEAs. They[48] found that the probably necessary requirements needed to form single-phase solid solutions are: $-16.25\ \text{kJ/mol} \le \Delta H_{\text{mix}}^{\text{liq}} \le +5\ \text{kJ/mol}$, $\delta \le 6\%$, $\Omega \ge 1$, $\eta \ge 0.19$, $\phi \ge 7.0$, $\varepsilon_{\text{R.M.S.}} \le 0.061$, and $E_2/E_0 \le 13.6 \times 10^{-4}$. However, these are not sufficient conditions since many multiphase compositions also satisfy these criteria.

The select empirical parameters of those predicted single-phase HEA compositions[30] are shown in Fig. 1, and all parameters evaluated in this work are summarized in Table SI (Supplementary Material). Clearly, the vast majority of the predicted compositions satisfy those reevaluated criteria by Gao et al.[48] The calculated $\Delta\chi$ values using the Pauling electronegativity are less than 0.36. Many compositions do not satisfy the $\Delta H_{\text{IM}}/\Delta H_{\text{mix}}^{\text{liq}} < \kappa_1^{\text{cr}}$ criterion.[15] Those compositions recommended by Troparevsky et al.[14] have a $\overline{\text{VEC}}$ greater than 7.43, suggesting that most of them either prefer the FCC or HCP structure as the main phase in their microstructures [Fig. 1(e)]. The average bulk and shear moduli were estimated using the ROM:

$$\bar{P} = \sum_i c_i P_i \quad , \tag{4}$$

where P_i refers to the properties of the ith element [lattice parameter (a), elastic constants (C_{ij}), bulk modulus (B), and shear modulus (G)], and $\bar{P}$ refers to the corresponding average value for the alloy. The result is shown in Fig. 1(f). The HEAs that comprise of alkali earth and/or rare earth elements are very soft since their shear and bulk moduli are very small, while other HEAs that contain high-melting transition metals have a significantly higher shear and bulk moduli.

B. CALPHAD predictions: new septenary, octonary, and ennead BCC HEAs

Figure 2 shows the calculated equilibrium phase mole fraction as a function of temperature for septenary CrMoNbTaTiVW, octonary CrMoNbReTaTiVW, and ennead CrFeMoNbReRuTaVW, using the TCNI8 database.[50] The insets are the nonequilibrium solidification using the Scheil–Gulliver models,[51,52] which assume equilibrium mixing in the liquid state and no diffusion in the solid state. Both the equilibrium and Scheil simulations predict the formation of a single BCC solid solution in CrMoNbTaTiVW and CrMoNbReTaTiVW, while formation of C14 and HCP phases in very small fractions toward the end of the Scheil solidification is predicted for CrFeMoNbReRuTaVW.

It has been proposed[30] that a stable single-phase solid solution in as-cast state is promoted when there is a wide temperature range (T_{rd}) between the solidus temperature (T_{sol}) and decomposition temperature (T_{dec}):

$$T_{\text{rd}} = (T_{\text{sol}} - T_{\text{dec}})/T_{\text{sol}} \ge 0.3 \quad . \tag{5}$$

The calculated T_{rd} parameters from the equilibrium thermodynamic calculation are 0.40, 0.43, and 0.29 for CrMoNbTaTiVW, CrMoNbReTaTiVW, and CrFeMoNbReRuTaVW, respectively. Both the Scheil simulations and the calculated T_{rd} values suggest that CrFeMoNbReRuTaVW may be on the verge of forming a single BCC phase in the as-cast condition.

IV. ENTROPY OF MIXING AND ENTROPY SOURCES

A. Entropy of mixing calculated from CALPHAD

The compositional dependences of the entropy of mixing for the FCC phase in the Co–Cr–Fe–Mn–Ni system and the BCC phase in the Mo–Nb–Ta–V–W

https://doi.org/10.1557/jmr.2017.366 Published online by Cambridge University Press

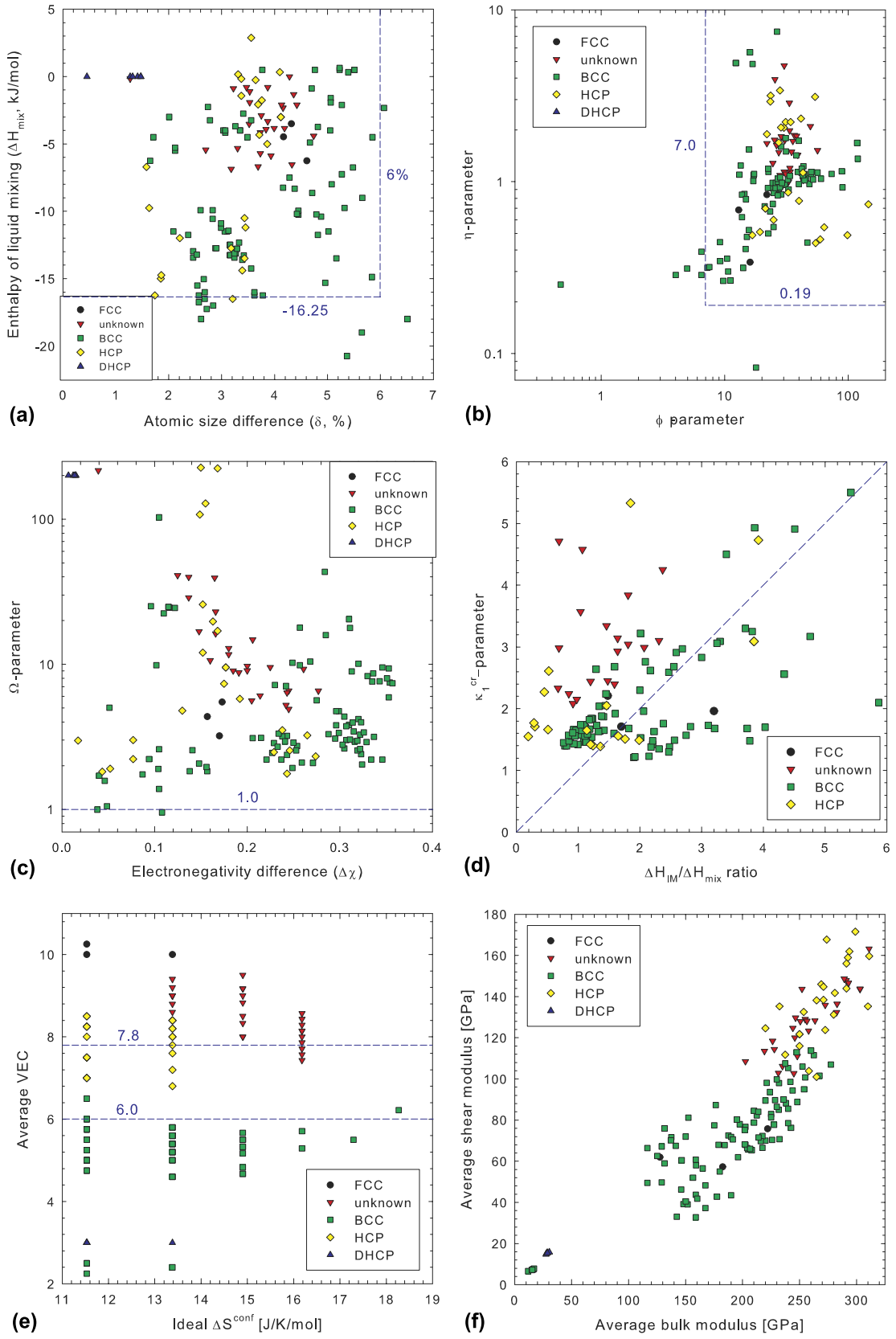


FIG. 1. Calculated empirical parameters for those predicted single-phase HEA compositions[14,30,39]: (a) $\Delta H_{\mathrm{mix}}^{\mathrm{liq}}$ versus δ, (b) η-parameter versus ϕ-parameter, (c) Ω-parameter versus $\Delta\chi$, (d) $\Delta H_{\mathrm{IM}}/\Delta H_{\mathrm{mix}}^{\mathrm{liq}}$ versus κ_1^{cr}, (e) $\overline{\mathrm{VEC}}$ versus $\Delta S_{\mathrm{ideal}}^{\mathrm{conf}}$, and (f) $\bar{B}$ versus $\bar{G}$. The marked threshold values are obtained from the work by Gao et al.[48]

https://doi.org/10.1557/jmr.2017.366 Published online by Cambridge University Press

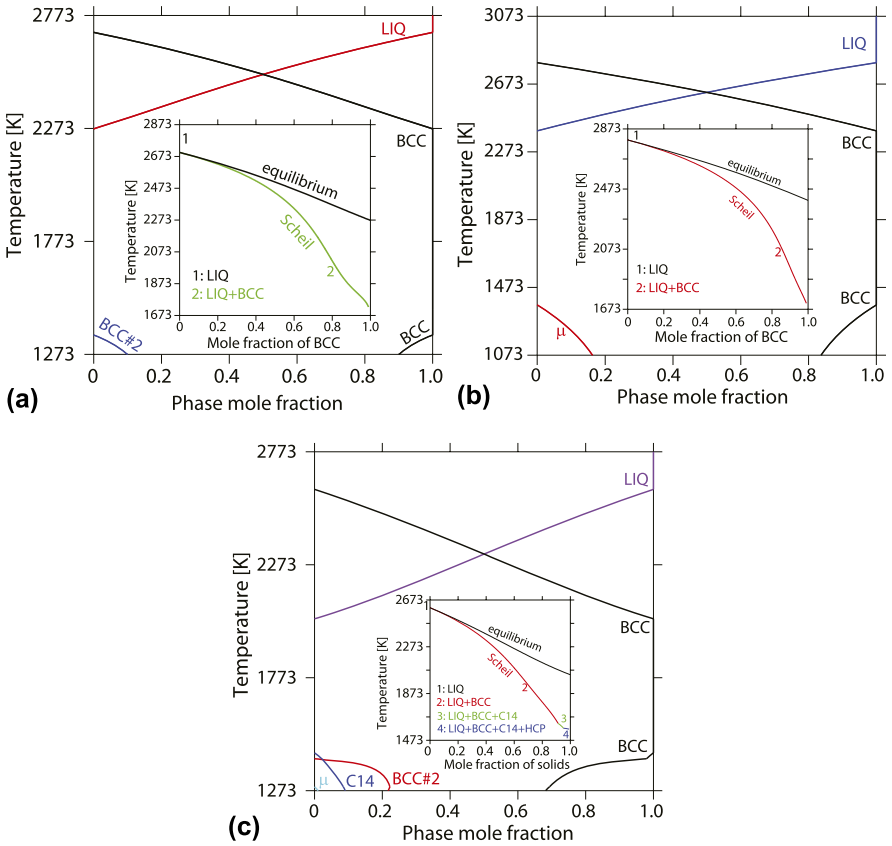


FIG. 2. Calculated equilibrium phase mole fraction as a function of temperature for (a) CrMoNbTaTiVW, (b) CrMoNbReTaTiVW, and (c) CrFeMoNbReRuTaVW, using the TCNI8 database. The insets are the corresponding Scheil simulations.

system at $T = 1273$ K are illustrated in Fig. 3 using the CALPHAD method. The ideal configurational entropies are also shown as a reference in dashed lines. Due to the presence of a short-range order, or segregation, and the contribution from the lattice phonon vibration, or magnetic contribution, the total entropy of mixing $\left(\Delta S^{\varphi}_{\mathrm{mix}}\right)$ for HEAs may not always follow ideal mixing and can cause positive or negative deviation from $-R\sum_i c_i \ln c_i$ (i.e., excess entropy). The excess entropy $\left({}^{\mathrm{ex}}S^{\varphi}_{\mathrm{mix}}\right)$ of a solution phase (φ) is calculated by subtracting the ideal configurational entropy from the total entropy of the alloy $\left(\Delta S^{\varphi}_{\mathrm{mix}}\right)$[28]:

$$ {}^{\mathrm{ex}}S^{\varphi}_{\mathrm{mix}} = \Delta S^{\varphi}_{\mathrm{mix}} + R\sum_i c_i \ln c_i \quad . \qquad (6) $$

The FCC phase in the Co–Cr–Fe–Mn–Ni system [Figs. 3(a) and 3(b)] exhibits a positive deviation from the ideal mixing and thus positive excess entropy for equal and near-equimolar compositions. The maximum excess entropy becomes smaller with increasing the number of components [Fig. 3(b)]. The compositions with the highest $\Delta S^{\mathrm{FCC}}_{\mathrm{mix}}$ also do not necessarily occur at the equimolar compositions. In contrast, the BCC phase in the Mo–Nb–Ta–V–W system [Figs. 3(c) and 3(d)] shows a negative deviation from the ideal mixing, and thus the negative excess entropy at equal and near-equimolar compositions except that the Mo–V binary shows an ideal mixing behavior [Fig. 3(d)]. At equimolar compositions, the calculated entropy of mixing for both FCC and BCC phases increases with increasing the number of components, suggesting the dominance of configurational entropy over other entropy sources at $T = 1273$ K. However, the contrasting behavior in the excess entropy between FCC and BCC structures indicates that the other entropy sources such as the vibrational entropy of mixing may also be important, as revealed from DFT calculations (see Sec. IV.B).

B. DFT calculations: enthalpy of formation and entropy sources

In general, SQS models tend to maximize random distributions of atoms in the lattice, but the permutation in the atomic position between elements may alter the local atomic environment and accordingly the fluctuation in the energy. The total number of atomic configurations for an HEA SQS model that result from atomic permutation scales up almost exponentially with increasing the number of equimolar components, and it is

https://doi.org/10.1557/jmr.2017.366 Published online by Cambridge University Press

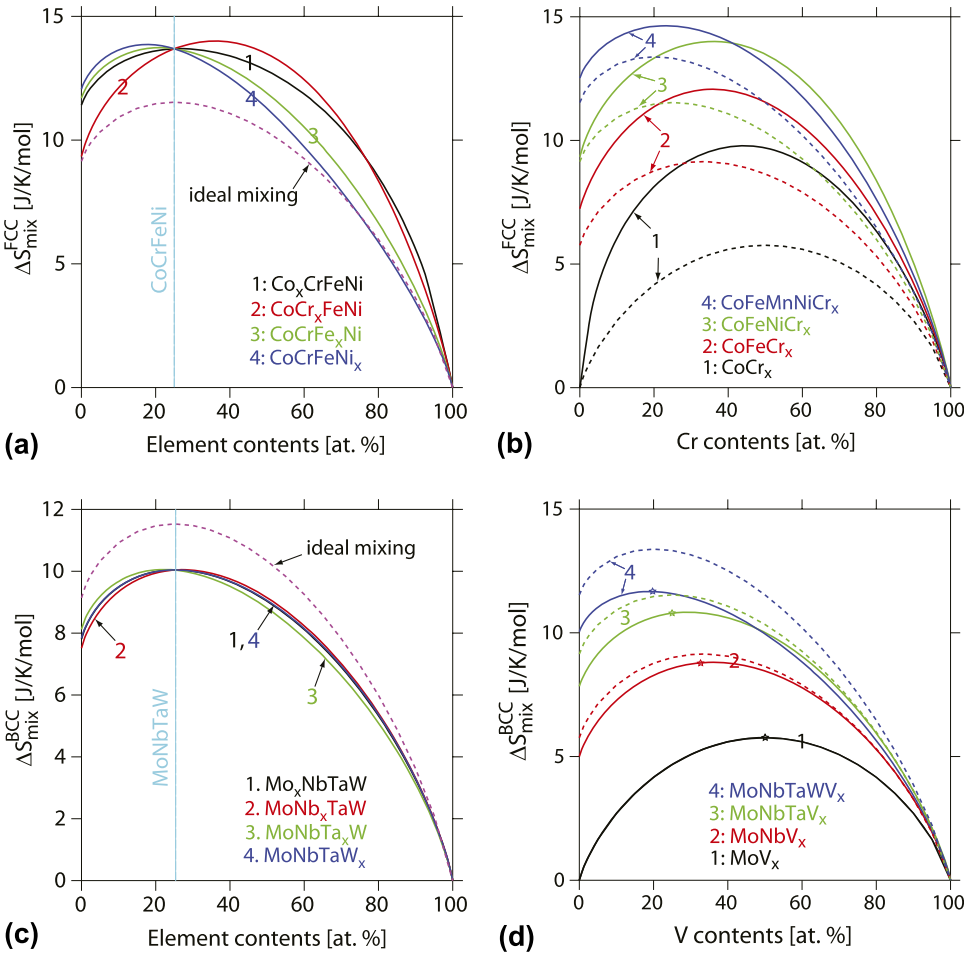


FIG. 3. Calculated total entropy of mixing at T = 1273 K using the TCNI8 database for: (a) the FCC phase in the Co–Cr–Fe–Ni system; (b) the FCC phase in the CoCr$_x$, CoFeCr$_x$, CoFeNiCr$_x$, and CoFeMnNiCr$_x$ systems; (c) the BCC phase in the Mo–Nb–Ta–W system; and (d) the BCC phase in the MoV$_x$, MoNbV$_x$, MoNbTaV$_x$, and MoNbTaWV$_x$ systems. The star symbols in (b) and (d) mark the equimolar compositions. The dashed curves represent the ideal mixing.

24 for an equimolar quaternary HEA (4! = 24) and 120 for an equimolar quinary HEA (5! = 120). To examine the effect of element permutation on the enthalpy of formation (ΔH_{SS}), DFT calculations were carried out on all 24 configurations of FCC CoCrFeNi, BCC MoNbTaW, and HCP CoOsReRu, and the results are shown in Fig. 4(a). The averaged ΔH_{SS} are 8.354 ± 0.266 kJ/mol, −7.407 ± 0.069 kJ/mol, and 2.724 ± 0.49 kJ/mol for CoCrFeNi, MoNbTaW, and CoOsReRu, respectively. Relatively speaking, CoOsReRu is a bit more sensitive to the atomic configuration than the other two structures, presumably due to the anisotropy of the HCP structure compared to the cubic structure. Other factors that may also contribute to the sensitivity with respect to the atomic configuration in SQS models are electronegativity, magnetism, and atomic size of the constituent elements. It can be assumed that this sensitivity may decrease with increasing the SQS cell size which, however, may increase the computing time substantially.

The calculated ΔH_{SS} for widely studied single-phase HEAs are shown in Fig. 4(b). Note that only one randomly chosen atomic configuration of the SQS model was used in the calculations (except CoCrFeNi, MoNbTaW, and CoOsReRu whose averaged ΔH_{SS} was used), so a small fluctuation in ΔH_{SS} is expected upon atomic permutation tests. For FCC and HCP HEAs, the calculated ΔH_{SS} is positive or close to zero. BCC AlNbTiV has the most negative ΔH_{SS} at −10.3 kJ/mol, followed by BCC MoNbTaW. Addition of HCP metals such as Hf, Ti, and Zr to BCC refectory metals causes a near-zero, or even positive, ΔH_{SS}.

The electronic DOS for FCC CoCrFeNi, BCC MoNbTaW, and HCP CoOsReRu is shown in Fig. 5. Integration of the difference between spin-up and spin-down electronic DOS gives rise to the magnetic moment, which is 0.62 ± 0.03 μ_B/atom for CoCrFeNi and 0.11 ± 0.02 μ_B/atom for CoOsReRu (here μ_B = Bohr magneton), averaged from total 24 atomic configurations. A clear pseudo-gap exists only for MoNbTaW,

https://doi.org/10.1557/jmr.2017.366 Published online by Cambridge University Press

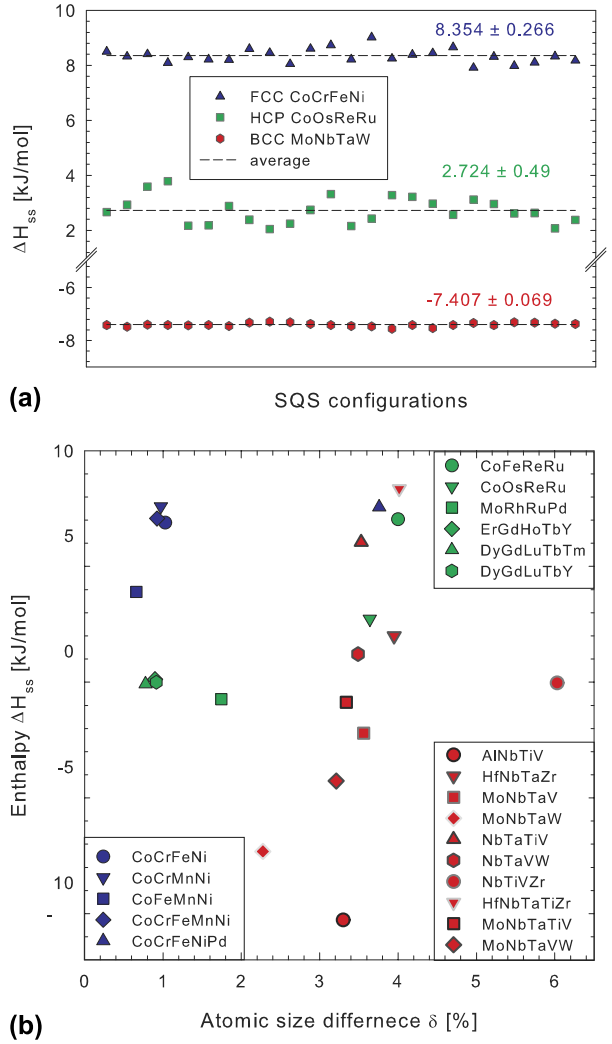


FIG. 4. (a) Enthalpy of formation (ΔH_{SS}) versus SQS configurations for FCC CoCrFeNi, BCC MoNbTaW, and HCP CoOsReRu. (b) DFT-calculated enthalpy of formation versus atomic size difference for various single-phase HEAs with the FCC, BCC, and HCP structures at zero temperature.

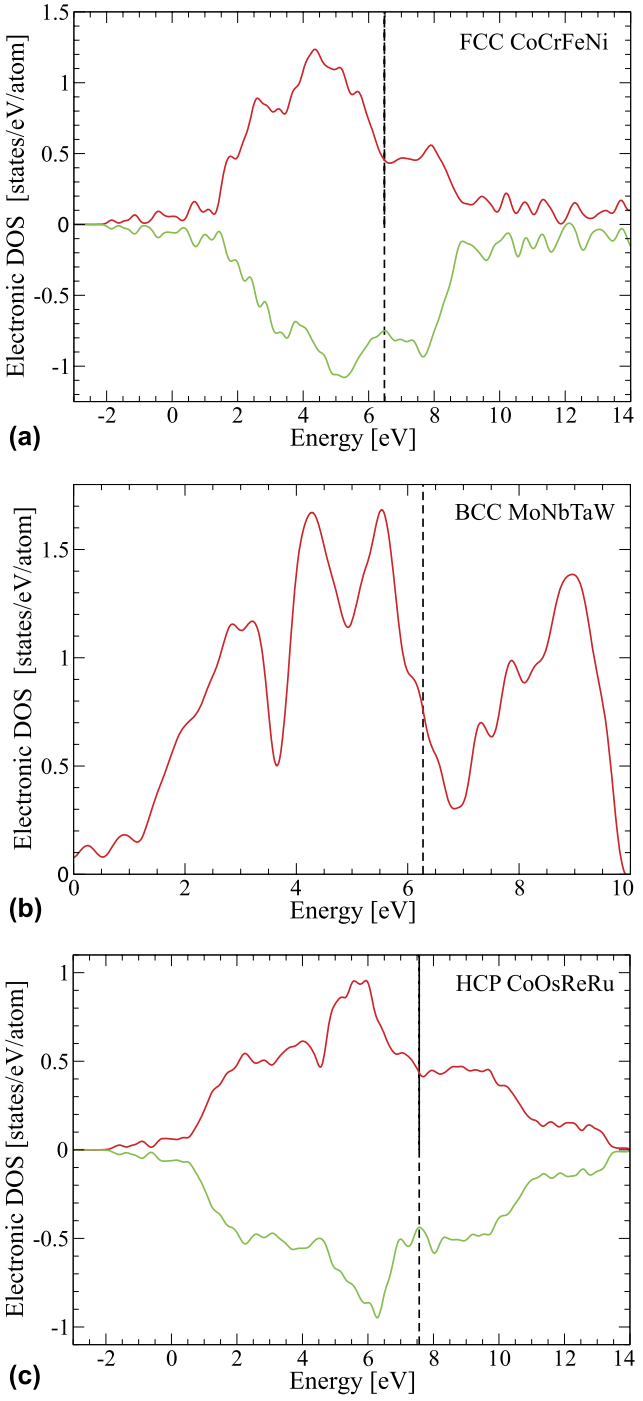


FIG. 5. DFT-calculated electronic DOS for (a) FCC CoCrFeNi, (b) BCC MoNbTaW, and (c) HCP CoOsReRu. The vertical dashed lines mark the Fermi level.

and the Fermi level sits on the left edge to the gap. Existence of a deep pseudo-gap of an alloy usually suggests thermodynamic stability, and this is consistent with the negative ΔH_{SS} of −7.407 kJ/mol for BCC MoNbTaW. Conversely, the Fermi levels of CoCrFeNi and CoOsReRu sit on (relatively speaking) a plateau with a low DOS.

The entropy sources of a solid solution phase may comprise contributions from the lattice vibration (S^{vib}), configuration (S^{conf}), electronic excitation (S^{elec}), and magnetic spin fluctuations (S^{mag}):

$$S^{total} = S^{vib} + S^{conf} + S^{elec} + S^{mag} \quad . \qquad (7)$$

Since the critical magnetic ordering temperatures for FCC CoCrFeNi and CoCrFeMnNi are well below room temperature,[53,54] it is sensible to assume that their magnetic entropy term should be temperature independent and thus can be ignored at $T \geq 293$ K for simplicity. The HCP CoOsReRu HEA was first suggested by Gao and Alman,[25] and there are no experiments reported yet.

Figure 6(a) presents the phonon DOS of FCC CoCrFeNi, BCC MoNbTaW, and HCP CoOsReRu.

https://doi.org/10.1557/jmr.2017.366 Published online by Cambridge University Press

Excellent agreement in the phonon DOS for CoCrFeNi with the experiment[53] is evident. At low energies (less than 10 meV), the phonon DOS is comparable for CoCrFeNi and CoOsReRu, but both are smaller than MoNbTaW. In contrast, the calculated vibrational heat capacity [C_V, see Fig. 6(b)] is very similar for all three alloys, although it is slightly larger for CoOsReRu and MoNbTaW than that for CoCrFeNi at $T \leq 400$ K. At higher temperatures, the vibrational C_V approaches the theoretical limit 3R.

Alloy entropies of mixing (ΔS_{mix}) are calculated by subtracting the composition–weighted total entropies of the constituent elements from the entropy of the alloy for total entropy, vibrational entropy, and electronic entropy, respectively. DFT-calculated total vibrational and electronic entropies for FCC CoCrFeNi, BCC MoNbTaW, and HCP CoOsReRu were reported elsewhere.[36,48] The vibrational entropies of pure elements of FCC Co, BCC Cr, antiferromagnetic FCC Fe, and FCC Ni were used for calculating the ΔS_{mix} of CoCrFeNi. FCC Cr was discarded because of the presence of 64 imaginary vibrational modes (out of a total of 324 modes) and its elastic instability.

The calculated ΔS_{mix} from various entropy sources for these HEAs are shown in Fig. 6(c). The calculated entropies of mixing for these three HEAs in descending

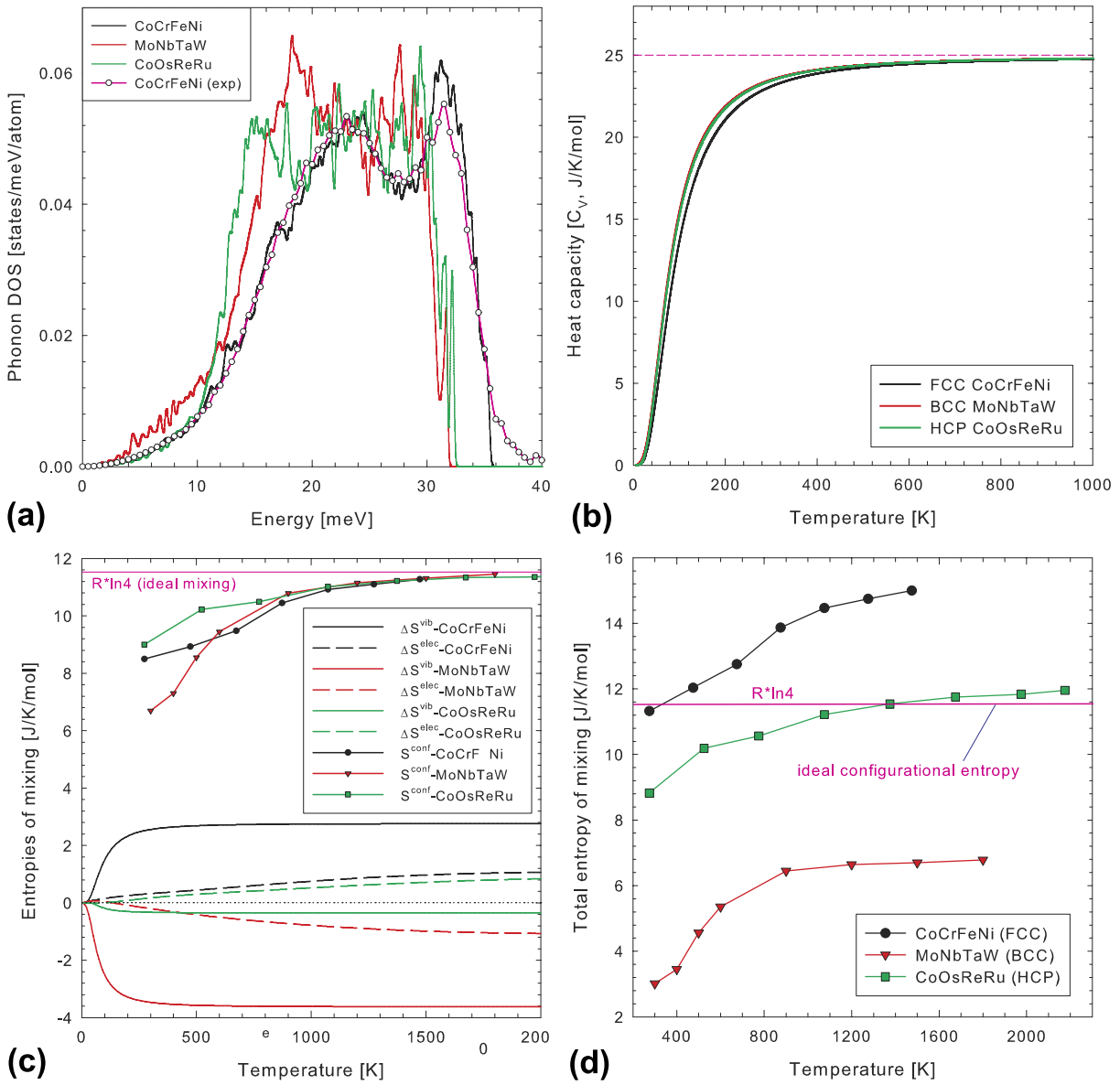


FIG. 6. (a) DFT-calculated vibrational DOS using the harmonic approximation. The experimental data for FCC CoCrFeNi was measured by Lucas et al.[53] (b) DFT-calculated vibrational heat capacity at a constant volume. (c) DFT- and MC/MD-predicted entropies of mixing from lattice configurations (S^{conf}), phonon vibrations (ΔS^{vib}_{mix}), and electron excitations (ΔS^{elec}_{mix}). (d) Total entropy of mixing based on (c).

https://doi.org/10.1557/jmr.2017.366 Published online by Cambridge University Press

order are: $S^{\text{conf}} \gg \left|\Delta S_{\text{mix}}^{\text{vib}}\right| \gg \left|\Delta S_{\text{mix}}^{\text{elec}}\right|$. At a temperature close to the solidus temperatures, the calculated S^{conf} is fairly close to their ideal value (R ln 4) and start to decrease very gradually until the temperature reaches 1100 K. At lower temperatures, S^{conf} decreases rapidly, signaling the development of chemical short-range order in the alloys. Note that S^{conf} at room temperature is much lower for MoNbTaW than for the others due to the tendency in forming the ordered BCC (i.e., B2) as revealed by Widom et al.[32,47] The vibrational entropies of mixing (ΔS^{vib}) approach constant values at temperatures above the Debye temperature (i.e., $T \geq \sim$400 K), namely, +2.8 J/K/mol, −3.6 J/K/mol, and −0.4 J/K/mol for CoCrFeNi, MoNbTaW, and CoOsReRu, respectively. This is because the heat capacities approach their classical limit at 3R. In contrast, the calculated $\Delta S_{\text{mix}}^{\text{elec}}$ values are close to zero. The sum of all entropy sources shows that the total entropy of the mixing in descending order for these alloys is: CoCrFeNi > CoOsReRu > MoNbTaW [Fig. 6(d)].

V. ELASTIC PROPERTIES

Single-crystal elastic constants (C_{ij}) are derived by performing six finite distortions of the lattice as implemented in VASP[55,56] through the basic elastic stress–strain relationship:

$$\sigma_i = \sum_{j=1}^{6} C_{ij}\varepsilon_j \quad , \tag{8}$$

where σ_i, ε_j, and C_{ij}, are the elastic stress, strain, and tensor in the Voigt notation, respectively. Since the local chemical environment in an SQS lattice may not be perfectly random or isotropic for HEAs, an averaging scheme proposed by Gao et al.[56] to obtain single-crystal C_{11}, C_{12}, and C_{44} for cubic structures was adopted in this work:

$$C_{11} = \frac{C_{11} + C_{22} + C_{33}}{3} \quad , \tag{9}$$

$$C_{12} = \frac{C_{12} + C_{23} + C_{13}}{3} \quad ,$$

$$C_{44} = \frac{C_{44} + C_{55} + C_{66}}{3} \quad .$$

The polycrystalline bulk modulus is determined by:

$$B = \frac{1}{3}(C_{11} + 2C_{22}) \quad . \tag{10}$$

The polycrystalline shear modulus (G) is estimated as the simple average of G_{V} and G_{R}, which is given by:

$$G_{\text{V}} = \frac{(C_{11} - C_{12} + 3C_{44})}{5} \quad ,$$
$$G_{\text{R}} = \frac{5(C_{11} - C_{12})C_{44}}{4C_{44} + 3(C_{11} - C_{12})} \quad . \tag{11}$$

The poisson's ratio (ν) of the alloy can be derived from the bulk modulus (B) and the shear modulus (G) of the alloy:

$$\nu = \frac{3B - 2G}{2(3B + G)} \quad . \tag{12}$$

The average Poisson's ratio ($\bar{\nu}$) of the alloy was estimated by:

$$\bar{\nu} = \frac{3\bar{B} - 2\bar{G}}{2(3\bar{B} + \bar{G})} \quad , \tag{13}$$

where $\bar{B}$ and $\bar{G}$ are the average bulk modulus and shear modulus of the alloy estimated using the ROM.

The necessary and sufficient conditions for cubic crystals to be mechanically stable are proposed by Born and Huang[57]:

$$C_{11} - C_{12} > 0;\ C_{11} + 2C_{12} > 0;\ C_{44} > 0 \quad . \tag{14}$$

Consequently, the Poisson's ratio of a mechanical stable crystal should be: $-1 < \nu < 0.5$. However, Feng and Widom[58] showed that elements Hf, Ti, and Zr in the BCC structure are mechanically unstable since their DFT calculations predict $C_{12} > C_{11}$. For consistency in the comparison, the lattice parameters and elastic properties of BCC Hf, Ti, and Zr calculated by Feng and Widom,[58] Tian et al.,[59] and Ge et al.[60] were used to calculate the average properties of BCC HEAs (see Table SII in Supplementary Material). Similarly, the present DFT work predicts the elastic constants of FCC Cr to be: C_{11} = 26 GPa, C_{12} = 348 GPa, C_{44} = −87 GPa, resulting in unphysical values of G = −112 GPa and ν = 0.78. In contrast, the calculated elastic properties of BCC Cr in the antiferromagnetic state are: C_{11} = 434 GPa, C_{12} = 59 GPa, C_{44} = 96 GPa, B = 184 GPa, G = 126 GPa, ν = 0.22, and they satisfy the stability criteria set by Eq. (14). Therefore, the mechanically stable BCC Cr is used instead to calculate the average properties of FCC CoCrFeNi and FCC CoCrFeMnNi in the present work (see Table SIII in Supplementary Material).

The lattice parameters and elastic properties of select equimolar HEAs that were computationally studied by Gao et al.,[36] Feng and Widom,[58] Tian et al.,[59] and Ge et al.,[60] were assessed in this work. Four ternary BCC, eight quaternary BCC, two quinary BCC, one quaternary FCC, and one quinary FCC equimolar alloys were studied. The elastic properties of single-phase HEAs

https://doi.org/10.1557/jmr.2017.366 Published online by Cambridge University Press

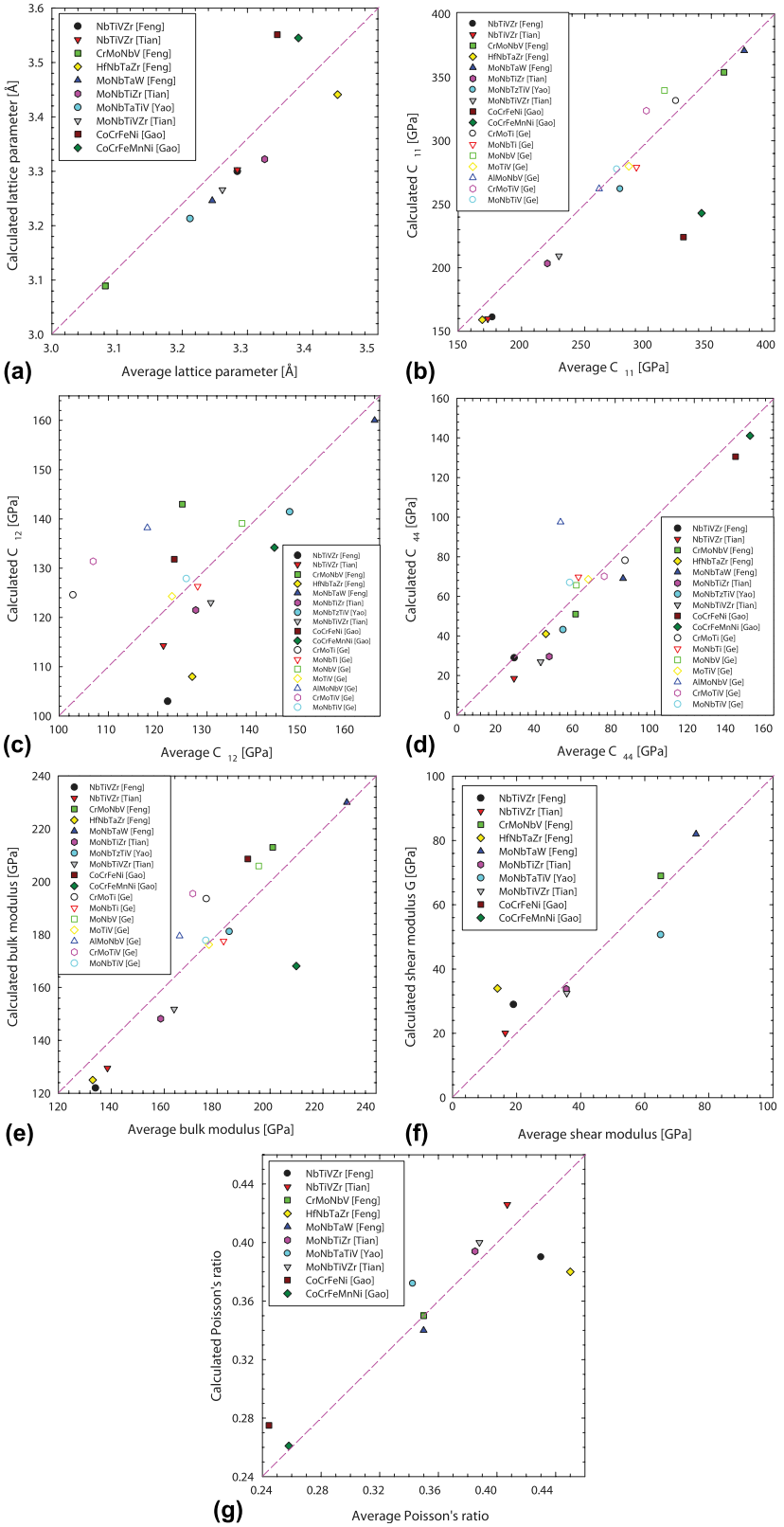


FIG. 7. Comparison between DFT calculations and the ROM in: (a) lattice parameter (a), (b–d) single-crystal elastic constants (C_{11}, C_{12}, and C_{44}), (e) polycrystalline bulk modulus (B), (f) polycrystalline shear modulus (G), and (g) polycrystalline Poisson's ratio (ν). The data shown are taken from the work by Gao et al.,[36] Feng and Widom,[58] Tian et al.,[59] and Ge et al.[60]

https://doi.org/10.1557/jmr.2017.366 Published online by Cambridge University Press

were previously reviewed by Gao et al.[36] and Tian et al.[35,61] The data are provided in Table SIV (Supplementary Material), and the comparison in the lattice parameters and elastic properties between DFT calculations and the ROM is shown in Fig. 7. For BCC HEAs, DFT calculations slightly underestimated the lattice parameter compared with the averaged values [Fig. 7(a)]. For FCC CoCrFeNi and CoCrFeMnNi, DFT calculations overestimated the lattice parameters compared with the averaged values presumably because the lattice parameter of BCC Cr with two atoms in the unit cell, which is significantly smaller than that of FCC Cr (see Table SIII), was used for the ROM. Excellent agreement in C_{11} between calculations and averages is observed except for the FCC HEAs [Fig. 7(b)] probably because the property of BCC Cr was used. The C_{12} values scatter much more widely than those of C_{11} or C_{44} [Figs. 7(b)–7(d)]. The distribution of B, G, and ν is close to the equality lines with a minor scatter [Figs. 7(e)–7(g)].

VI. DISCUSSION

Predicting the formation of single-phase HEA compositions has been an intense research topic[3,6–36,62] and yet the total number of single-phase HEAs confirmed by experiments is still very limited.[30,48] Single-phase HEAs with the total number of principal elements greater than five are very scarce, including senary compositions (HfNbTaTiVZr,[21] MoNbTaTiVW,[29] CrMoNbTaVW,[29] and MoNbReTaVW[38]) and septenary compositions (MoNbReTaTiVW,[38] CrMoNbReTaVW,[63] and CuIrNiPdPtRh[64]). Strictly speaking, formation of single-phase HEAs is the direct consequence of multiphase competition as a function of temperature and composition toward minimizing the total Gibbs free energy of the system, and thus the CALPHAD method is the ideal tool for tackling phase stability in multicomponent systems such as HEAs. However, most commercial databases are intended for compositions that are enriched in the principal element, and thus simple extrapolation to the compositional center of a phase diagram may produce inaccurate or even wrong predictions. Other databases that are dedicated to HEAs may not cover all constituent binaries and ternaries in their entire composition and temperature ranges. Other roadblocks to developing a reliable database include lack of sufficient experimental data and/or the lack of physically meaningful descriptions for those hypothetical phases such as endmembers and antiphases.[28,48]

Gao et al.[48] also analyzed the weakness of those empirical parameters, which included the underlying hypotheses, oversimplified treatment of the entropy of mixing for the solution phase, and the oversimplified treatment of the enthalpy of intermetallic phases. However, if the CALPHAD databases are not available or do not cover all the binaries and ternaries, phase diagram inspection or employing available empirical thermophysical parameters become especially important in the quick selection of promising elements that are most likely to promote the formation of solid solution phases as opposed to intermetallic phases. Gao[30] first summarized that those experimentally confirmed single-phase HEAs exhibit either an isomorphous solid solution (e.g., the Nb–Mo–Ta–W and Hf–Nb–Ta–Ti–Zr systems) or quite large terminal solubilities (e.g., Co–Fe–Mn–Ni system) in their constituent binaries and ternaries. Gao[30] further highlighted three types of solid solutions in a phase diagram that are important for HEA formation: (i) Isomorphous solid solution (e.g., the FCC phase in the Co–Ni binary and the HCP phase in the Re–Ru binary), (ii) extended terminal solid solubility (e.g., the BCC and HCP phases in the Cr–Ru binary), and (iii) intermediate solid solution (e.g., the HCP phase in the Cr–Rh binary).

Good agreement in predicting the entropy of mixing between DFT calculations and CALPHAD was obtained in the present study. More importantly, DFT calculations illuminated the entropy sources of HEAs and revealed that the positive vibrational entropy of mixing in FCC CoCrFeNi mainly contributes to its positive excess entropy. Alternatively, the negative vibrational entropy of mixing in BCC MoNbTaW mainly contributes to its negative excess entropy. The sign of the vibrational entropy of mixing [Fig. 5(c)] for FCC CoCrFeNi and BCC MoNbTaW seems to coincide with the sign of their enthalpies of formation [Fig. 4(b)]. The presence of a strong short-range order in BCC MoNbTaW[32,33] causes a larger negative enthalpy of formation, decreases the average atomic volume, and, hence, promotes an increase in the phonon vibrational frequency. Conversely, a larger positive enthalpy of formation in FCC CoCrFeNi may enlarge the overall bond length and, hence, increase the average atomic volume, while potentially decreasing the phonon vibrational frequency. The enthalpy of formation of HCP CoOsReRu is close to zero, and this suggests a negligible bond formation in the alloy, which may have little impact on the phonon vibrational frequency. Indeed, the calculated vibrational entropy of mixing is zero for HCP CoOsReRu.

At $T > 400$ K, the calculated vibrational entropy of mixing is +2.8, −3.6, and −0.3 J/K/mol for FCC CoCrFeNi, BCC MoNbTaW, and HCP CoOsReRu, respectively. Calculated entropies of mixing for these three HEAs in descending order are: $S^{\mathrm{conf}} \gg \left|\Delta S_{\mathrm{mix}}^{\mathrm{vib}}\right| \gg \left|\Delta S_{\mathrm{mix}}^{\mathrm{elec}}\right|$. Although the calculated configurational entropies approach the theoretical limit at high temperatures close to their melting points, developing a short-range order can cause a sharp decrease in the configurational entropy at low temperatures. As a result, the total entropy of mixing of an HEA depends on the configurational entropy as well as the vibrational entropy of mixing and

https://doi.org/10.1557/jmr.2017.366 Published online by Cambridge University Press

is more sensitive to temperature at intermediate and low temperatures. The total entropies of mixing (i.e., $\Delta S_{mix}^{vib} + \Delta S_{mix}^{elec} + S^{conf}$) were observed to trend in the following manner: CoCrFeNi > CoOsReRu > MoNbTaW at $T \geq 300$ K.

The solid solution stabilization by phonon vibration was also reported by Fultz et al.[65] who measured ΔS_{mix}^{vib} to be +1.17, +1.67, and +1.78 J/K/mol for disordered BCC solid solution alloys $Fe_{70}Cr_{30}$, $Fe_{53}Cr_{47}$, and $Fe_{30}Cr_{70}$, respectively. However, it is generally not obvious whether a chemical disordering causes a positive or negative vibrational entropy of mixing or whether a disordered alloy will exhibit a greater vibrational entropy than its ordered form. The vibrational entropy of mixing of an alloy may depend on the crystal structure, bonding, and enthalpy of the alloy, as well as the molar volumes and structures of the constituent elements.[66] For example, Munoz et al.[67] found that the chemical ordering in the B2 structure increases the vibrational entropy by 1.83 J/K/mol, compared to the disordered B2 FeV alloy.

Elastic properties (such as elastic constants and bulk/shear moduli) of a solid solution primarily depend on the interatomic interactions among constituent elements. Intuitively speaking, electron hybridization may result in a strong attractive interaction, and accordingly, a shortened bond length, and a negative enthalpy of formation (ΔH_{SS}). Conversely, repulsive interaction may result in a positive enthalpy of formation. However, for BCC MoNbTaW that has an ΔH_{SS} of −7.4 kJ/mol, its lattice parameter, elastic constants, and average bulk and shear moduli agree well with the averages estimated from ROM. To further examine the distribution of the calculated properties (a, C_{11}, C_{12}, C_{44}, B, G, and ν) with respect to the averaged values from ROM, the change in the properties in percentage is shown in Fig. 8. The maximum ranges in $\Delta P/P_{avg}$ are: 0.6% for a except 6.1% for CoCrFeNi and 4.9% for CoCrFeMnNi, 32% for C_{11}, 23% for C_{12}, 86% for C_{44}, 20% for B, 28% for G except extreme cases (143% for HfNbTaZr, and 53% for NbTiVZr), and 16% for ν. To make a meaningful comparison with respect to the averaged values, the properties of the pure elements are in the same crystal structure as the alloy should be used. However, certain elements are mechanically unstable in certain structures, such as FCC Cr and BCC Hf/Ti/Zr, and thus, it is controversial whether it is appropriate to use their properties, although seemingly unphysical, to calculate averaged properties via the ROM.

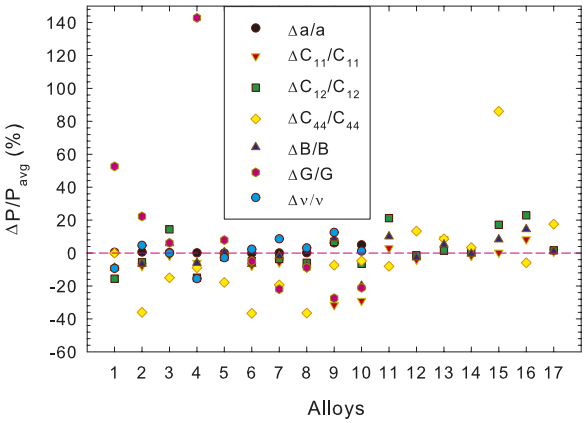


FIG. 8. Distribution in the change of calculated properties (a, C_{11}, C_{12}, C_{44}, B, G, and ν) with respect to the averaged properties. The alloy number is provided in the Table SIV Supplementary Material.

VII. CONCLUSIONS

This work evaluated the empirical thermo-physical parameters for hundreds of single-phase HEAs that were predicted using empirical parameters, CALPHAD, and phase diagram inspections. New septenary, octonary, and ennead BCC refractory HEAs were suggested. Entropy of mixing for three quaternary HEAs were modeled using CALPHAD, DFT, and MC/MD methods. The elastic properties of HEAs were evaluated. The following conclusions were reached:

(1) The vast majority of those predicted single-phase HEAs[30] satisfy the reevaluated empirical rules by Gao et al.[48] except the $\Delta H_{IM}/\Delta H_{mix}^{liq} < \kappa_1^{cr}$ criterion.[15] However, whether they form a single-phase solid solution awaits future experiment examination.

(2) Calculated $\overline{VEC}$ values hypothesize that the majority of the alloys suggested by Troparevsky et al.[14] may have the FCC or HCP structures as the main phase in the microstructure.

(3) Equilibrium calculations, Sheil simulations, and T_{rd} parameters using the TCNI8 database suggest that septenary CrMoNbTaTiVW and octonary CrMoNbReTaTiVW likely form BCC HEAs while ennead CrFeMoNbReRuTaVW may be on the border between the single-phase and multiphase.

(4) The TCNI8 database predicts a total entropy of mixing of 13.7 J/K/mol for FCC CoCrFeNi and 10.4 J/K/mol for BCC MoNbTaW at $T = 1273$ K, which corresponds to an excess entropy of +2.2 and −1.2 J/K/mol, respectively.

(5) DFT-calculated averaged enthalpy of formation for FCC CoCrFeNi, BCC MoNbTaW, and HCP CoOsReRu is 8.354 ± 0.266 kJ/mol, −7.407 ± 0.069 kJ/mol, and 2.724 ± 0.49 kJ/mol, respectively, resulting from 24 atomic configurations due to permutation between elements.

(6) The DFT-calculated enthalpy of formation of twenty-one single-phase solid solution HEAs are: $-10.3 \text{ kJ/mol} < \Delta H_{SS} < +8.4 \text{ kJ/mol}$.

(7) Calculated configurational entropies (S^{conf}) for CoCrFeNi, MoNbTaW, and CoOsReRu alloys were

https://doi.org/10.1557/jmr.2017.366 Published online by Cambridge University Press

fairly equivalent to their ideal value (R ln 4) at temperatures close to their solidus temperatures. However, S^{conf} at room temperature is much lower for MoNbTaW than the others due to the tendency in forming the ordered BCC (i.e., B2) as revealed by Widom et al.[32,47]

(8) DFT-calculated phonon DOS for FCC CoCrFeNi is in excellent agreement with the experiment by Lucas et al.[53] At $T > 400$ K, the calculated vibrational entropy of the mixing is +2.8, −3.6, and −0.3 J/K/mol for FCC CoCrFeNi, BCC MoNbTaW, and HCP CoOsReRu, respectively. Calculated entropies of mixing for these three HEAs in descending order are: $S^{conf} \gg |\Delta S_{mix}^{vib}| \gg |\Delta S_{mix}^{elec}|$.

(9) The DFT calculations illuminate the entropy sources of HEAs and reveal that the positive vibrational entropy of mixing in FCC CoCrFeNi mainly contributes to its positive excess entropy while the negative vibrational entropy of mixing in BCC MoNbTaW mainly contributes to its negative excess entropy.

(10) The total entropies of mixing (i.e., $\Delta S_{mix}^{vib} + \Delta S_{mix}^{elec} + S^{conf}$) were observed to trend in the following manner: CoCrFeNi > CoOsReRu > MoNbTaW.

(11) The maximum ranges in the properties with respect to the averaged values estimated from the ROM (i.e., $\Delta P/P_{avg}$) are: 0.6% for the lattice parameter a except 6.1% for CoCrFeNi and 4.9% for CoCrFeMnNi, 32% for C_{11}, 23% for C_{12}, 86% for C_{44}, 20% for the bulk modulus B, 28% for the shear modulus G except for the extreme cases (143% for HfNbTaZr and 53% for NbTiVZr), and 16% for the Poisson's ratio ν.

(12) The uncertainties in the elastic properties for certain elements that are mechanically unstable in certain crystal structures (e.g., FCC Cr, BCC Hf/Ti/Zr) may lead to biased results when estimating the average properties using the ROM (e.g., using FCC Cr versus BCC Cr, using BCC Hf/Ti/Zr versus HCP Hf/Ti/Zr).

DISCLAIMER

The computational modeling work presented in the article is a project that was funded by the Department of Energy, National Energy Technology Laboratory, an agency of the United States Government, through a support contract with AECOM. Neither the United States Government nor any agency thereof, nor any of their employees, nor AECOM, nor any of their employees, make any warranty, expressed or implied, or assumes any legal liability or responsibility for the accuracy, completeness, or usefulness of any information, apparatus, product, or process disclosed or represents that its use would not infringe privately owned rights. Reference herein to any specific commercial product, process, or service by trade name, trademark, manufacturer, or otherwise, does not necessarily constitute or imply its endorsement, recommendation or favoring by the United States Government or any agency thereof. The views and opinions of authors expressed herein do not necessarily state or reflect those of the United States Government or any agency thereof.

ACKNOWLEDGMENTS

This work was carried out in support of the Cross-Cutting Technologies Program at the National Energy Technology Laboratory (NETL), managed by Robert Romanosky (Technology Manager). The Research was executed through NETL's Research and Innovation Center's Innovative Process Technologies (IPT) Field Work Proposal. Research performed by AECOM Staff was conducted under the RES contract DE-FE-0004000. L.Z. Ouyang acknowledges support by DE-FE-0011549 and DE-NA0002630. Work at Carnegie Mellon was supported under grant DE-SC0014506.

REFERENCES

1. J.W. Yeh, S.K. Chen, S.J. Lin, J.Y. Gan, T.S. Chin, T.T. Shun, C.H. Tsau, and S.Y. Chang: Nanostructured high-entropy alloys with multiple principal elements: Novel alloy design concepts and outcomes. *Adv. Eng. Mater.* **6**, 299 (2004).
2. B. Cantor, I.T.H. Chang, P. Knight, and A.J.B. Vincent: Microstructural development in equiatomic multicomponent alloys. *Mater. Sci. Eng., A* **375–377**, 213 (2004).
3. Y. Zhang, T.T. Zuo, Z. Tang, M.C. Gao, K.A. Dahmen, P.K. Liaw, and Z.P. Lu: Microstructures and properties of high-entropy alloys. *Prog. Mater. Sci.* **61**, 1 (2014).
4. M.C. Gao, J.W. Yeh, P.K. Liaw, and Y. Zhang: *High-Entropy Alloys: Fundamentals and Applications*, 1st ed. (Springer International Publishing, Cham, 2016); p. 516.
5. D.B. Miracle and O.N. Senkov: A critical review of high entropy alloys and related concepts. *Acta Mater.* **122**, 448 (2017).
6. Y. Zhang, Y.J. Zhou, J.P. Lin, G.L. Chen, and P.K. Liaw: Solid-solution phase formation rules for multi-component alloys. *Adv. Eng. Mater.* **10**, 534 (2008).
7. Y. Zhang, Z.P. Lu, S.G. Ma, P.K. Liaw, Z. Tang, Y.Q. Cheng, and M.C. Gao: Guidelines in predicting phase formation of high-entropy alloys. *MRS Commun.* **4**, 57 (2014).
8. S. Guo, C. Ng, J. Lu, and C.T. Liu: Effect of valence electron concentration on stability of fcc or bcc phase in high entropy alloys. *J. Appl. Phys.* **109**, 103505 (2011).
9. S. Fang, X. Xiao, L. Xia, W. Li, and Y. Dong: Relationship between the widths of supercooled liquid regions and bond parameters of Mg-based bulk metallic glasses. *J. Non-Cryst. Solids* **321**, 120 (2003).
10. Y.F. Ye, Q. Wang, J. Lu, C.T. Liu, and Y. Yang: Design of high entropy alloys: A single-parameter thermodynamic rule. *Scr. Mater.* **104**, 53 (2015).
11. Y.F. Ye, C.T. Liu, and Y. Yang: A geometric model for intrinsic residual strain and phase stability in high entropy alloys. *Acta Mater.* **94**, 152 (2015).
12. Z.J. Wang, W.F. Qiu, Y. Yang, and C.T. Liu: Atomic-size and lattice-distortion effects in newly developed high-entropy alloys with multiple principal elements. *Intermetallics* **64**, 63 (2015).
13. D.J.M. King, S.C. Middleburgh, A.G. McGregor, and M.B. Cortie: Predicting the formation and stability of single phase high-entropy alloys. *Acta Mater.* **104**, 172 (2016).
14. M.C. Troparevsky, J.R. Morris, P.R.C. Kent, A.R. Lupini, and G.M. Stocks: Criteria for predicting the formation of single-phase high-entropy alloys. *Phys. Rev. X* **5**, 011041 (2015).

https://doi.org/10.1557/jmr.2017.366 Published online by Cambridge University Press

15. O.N. Senkov and D.B. Miracle: A new thermodynamic parameter to predict formation of solid solution or intermetallic phases in high entropy alloys. *J. Alloys Compd.* **658**, 603 (2016).
16. M.G. Poletti and L. Battezzati: Electronic and thermodynamic criteria for the occurrence of high entropy alloys in metallic systems. *Acta Mater.* **75**, 297 (2014).
17. I. Toda-Caraballo and P.E.J. Rivera-Diaz-del-Castillo: A criterion for the formation of high entropy alloys based on lattice distortion. *Intermetallics* **71**, 76 (2016).
18. S. Guo: Phase selection rules for cast high entropy alloys: An overview. *Mater. Sci. Technol.* **31**, 1223 (2015).
19. M.C. Gao, C.S. Carney, Ö.N. Doğan, P.D. Jablonksi, J.A. Hawk, and D.E. Alman: Design of refractory high-entropy alloys. *JOM* **67**, 2653 (2015).
20. B. Zhang, M.C. Gao, Y. Zhang, and S.M. Guo: Senary refractory high-entropy alloy Cr_xMoNbTaVW. *CALPHAD* **51**, 193 (2015).
21. M.C. Gao, B. Zhang, S. Yang, and S.M. Guo: Senary refractory high-entropy alloy HfNbTaTiVZr. *Metall. Mater. Trans. A* **47**, 3333 (2016).
22. H.W. Yao, J.W. Qiao, M.C. Gao, J.A. Hawk, S.G. Ma, H.F. Zhou, and Y. Zhang: NbTaV–(Ti,W) refractory high entropy alloys. *Mater. Sci. Eng., A* **674**, 203 (2016).
23. H.W. Yao, J.W. Qiao, M.C. Gao, J.A. Hawk, S.G. Ma, and H.F. Zhou: MoNbTaV medium-entropy alloy. *Entropy* **18**, 189 (2016).
24. C. Zhang, F. Zhang, S.L. Chen, and W.S. Cao: Computational thermodynamics aided high-entropy alloy design. *JOM* **64**, 839 (2012).
25. M.C. Gao and D.E. Alman: Searching for next single-phase high-entropy alloy compositions. *Entropy* **15**, 4504 (2013).
26. F. Zhang, C. Zhang, S.L. Chen, J. Zhu, W.S. Cao, and U.R. Kattner: An understanding of high entropy alloys from phase diagram calculations. *CALPHAD* **45**, 1 (2014).
27. O.N. Senkov, J.D. Miller, D.B. Miracles, and C. Woodward: Accelerated exploration of multi-principal element alloys for structural applications. *CALPHAD* **50**, 32 (2015).
28. C. Zhang and M.C. Gao: CALPHAD modeling of high-entropy alloys. In *High-Entropy Alloys: Fundamentals and Applications*, M.C. Gao, J.W. Yeh, P.K. Liaw, and Y. Zhang, eds. (Springer International Publishing, Cham, 2016); p. 399.
29. B. Zhang, M.C. Gao, Y. Zhang, S. Yang, and S.M. Guo: Senary refractory high-entropy alloy MoNbTaTiVW. *Mater. Sci. Technol.* **31**, 1207 (2015).
30. M.C. Gao: Design of high-entropy alloys. In *High-Entropy Alloys: Fundamentals and Applications*, M.C. Gao, J.W. Yeh, P.K. Liaw, and Y. Zhang, eds. (Springer International Publishing, Cham, 2016); p. 369.
31. M.C. Gao, B. Zhang, S.M. Guo, J.W. Qiao, and J.A. Hawk: High-entropy alloys in hexagonal close packed structure. *Metall. Mater. Trans. A* **47**, 3322 (2016).
32. M. Widom, W.P. Huhn, S. Maiti, and W. Steurer: Hybrid Monte Carlo/molecular dynamics simulation of a refractory metal high entropy alloy. *Metall. Mater. Trans. A* **45**, 196 (2014).
33. M. Widom: Prediction of structure and phase transformations. In *High-Entropy Alloys: Fundamentals and Applications*, M.C. Gao, J.W. Yeh, P.K. Liaw, and Y. Zhang, eds. (Springer International Publishing, Cham, 2016); p. 267.
34. F.Y. Tian, L. Delczeg, N.X. Chen, L.K. Varga, J. Shen, and L. Vitos: Structural stability of $NiCoFeCrAl_x$ high-entropy alloy from ab initio theory. *Phys. Rev. B* **88**, 085128 (2013).
35. F.Y. Tian, Y. Wang, D.L. Irving, and L. Vitos: Applications of coherent potential approximation to HEAs. In *High-Entropy Alloys: Fundamentals and Applications*, M.C. Gao, J.W. Yeh, P.K. Liaw, and Y. Zhang, eds. (Springer International Publishing, Cham, 2016); p. 299.
36. M.C. Gao, C. Niu, C. Jiang, and D.L. Irving: Applications of special quasi-random structures to high-entropy alloys. In *High-Entropy Alloys: Fundamentals and Applications*, M.C. Gao, J.W. Yeh, P.K. Liaw, and Y. Zhang, eds. (Springer International Publishing, Cham, 2016); p. 333.
37. D. Ma, B. Grabowski, F. Kormann, J. Neugebauer, and D. Raabe: Ab initio thermodynamics of the CoCrFeMnNi high entropy alloy: Importance of entropy contributions beyond the configurational one. *Acta Mater.* **100**, 90 (2015).
38. H. Bei: Multi-component solid solution alloys having high mixing entropy. USPC, No. US20130108502 A1, UT-BATTELLE, LLC, Oak Ridge, TN, Knoxville, 2013.
39. O.N. Senkov, J.D. Miller, D.B. Miracle, and C. Woodward: Accelerated exploration of multi-principal element alloys with solid solution phases. *Nat. Commun.* **6**, 6529 (2015).
40. G. Kresse and J. Hafner: Ab initio molecular dynamics for liquid metals. *Phys. Rev. B* **47**, 558 (1993).
41. G. Kresse and J. Furthmüller: Efficient iterative schemes for ab initio total-energy calculations using a plane-wave basis set. *Phys. Rev. B* **54**, 11169 (1996).
42. P.E. Blochl: Projector augmented-wave method. *Phys. Rev. B* **50**, 17953 (1994).
43. J.P. Perdew, K. Burke, and M. Ernzerhof: Generalized gradient approximation made simple. *Phys. Rev. Lett.* **77**, 3865 (1996).
44. S.H. Wei, L.G. Ferreira, J.E. Bernard, and A. Zunger: Electronic properties of random alloys: Special quasirandom structures. *Phys. Rev. B* **42**, 9622 (1990).
45. A. Zunger, S.H. Wei, L.G. Ferreira, and J.E. Bernard: Special quasirandom structures. *Phys. Rev. Lett.* **65**, 353 (1990).
46. H.J. Monkhorst and J.D. Pack: Special points for brillouin-zone integrations. *Phys. Rev. B* **13**, 5188 (1976).
47. W.P. Huhn and M. Widom: Prediction of A2 to B2 phase transition in the high-entropy alloy Mo–Nb–Ta–W. *JOM* **65**, 1772 (2013).
48. M.C. Gao, C. Zhang, P. Gao, F. Zhang, L.Z. Ouyang, M. Widom, and J.A. Hawk: Thermodynamics of concentrated solid solution alloys. *Curr. Opin. Solid State Mater. Sci.* (2017). (in press). doi: https://doi.org/10.1016/j.cossms.2017.08.001.
49. H. Ackermann, G. Inden, and R. Kikuchi: Tetrahedron approximation of the cluster variation method for bcc alloys. *Acta Metall.* **37**, 1 (1989).
50. B. Sundman, B. Jansson, and J.O. Andersson: The Thermo-Calc databank system. *CALPHAD* **9**, 153 (1985).
51. G.H. Gulliver: The quantitative effect of rapid cooling upon the constitution of binary alloys. *J. Inst. Met.* **9**, 120 (1913).
52. E. Scheil: Comments on the layer crystal formation. *Z. Metallkd.* **34**, 70 (1942).
53. M.S. Lucas, L. Mauger, J.A. Munoz, Y. Xiao, A.O. Sheets, S.L. Semiatin, J. Horwath, and Z. Turgut: Magnetic and vibrational properties of high-entropy alloys. *J. Appl. Phys.* **109**, 07E307 (2011).
54. M.S. Lucas, D. Belyea, C. Bauer, N. Bryant, E. Michel, Z. Turgut, S.O. Leontsev, J. Horwath, S.L. Semiatin, M.E. McHenry, and C.W. Miller: Thermomagnetic analysis of $FeCoCr_xNi$ alloys: Magnetic entropy of high-entropy alloys. *J. Appl. Phys.* **113**, 17A923 (2013).
55. Y. Le Page and P. Saxe: Symmetry-general least-squares extraction of elastic data for strained materials from ab initio calculations of stress. *Phys. Rev. B* **65**, 104104 (2002).
56. M.C. Gao, Y. Suzuki, H. Schweiger, Ö.N. Doğan, J. Hawk, and M. Widom: Phase stability and elastic properties of Cr–V alloys. *J. Phys.: Condens. Matter* **25**, 075402 (2013).
57. M. Born and K. Huang: *Dynamical Theory of Crystal Lattices*, 1st ed. (Clarendon Press, Oxford, 1954).

https://doi.org/10.1557/jmr.2017.366 Published online by Cambridge University Press

58. B. Feng and M. Widom: Elastic stability and lattice distortion of refractory high entropy alloys. *Mater. Chem. Phys.* (2017). (in press). doi: https://doi.org/10.1016/j.matchemphys.2017.06.038.
59. L.Y. Tian, G. Wang, J.S. Harris, D.L. Irving, J. Zhao, and L. Vitos: Alloying effect on the elastic properties of refractory high-entropy alloys. *Mater. Des.* **114**, 243 (2017).
60. H.J. Ge, F.Y. Tian, and Y. Wang: Elastic and thermal properties of refractory high-entropy alloys from first-principles calculations. *Comput. Mater. Sci.* **128**, 185 (2017).
61. F.Y. Tian, L.K. Varga, J. Shen, and L. Vitos: Calculating elastic constants in high-entropy alloys using the coherent potential approximation: Current issues and errors. *Comput. Mater. Sci.* **111**, 350 (2016).
62. Z. Wang, S. Guo, and C.T. Liu: Phase selection in high-entropy alloys: From nonequilibrium to equilibrium. *JOM* **66**, 1966 (2014).
63. B.L. Zhang, Y. Mu, M.C. Gao, W.J. Meng, and S.M. Guo: On single-phase status and segregation of an as-solidified septenary refractory high entropy alloy. *MRS Commun.* **7**, 78 (2017).
64. S.W. Sohn, Y.H. Liu, J.B. Liu, P. Gong, S. Prades-Rodel, A. Blatter, B.E. Scanley, C.C. Broadbridge, and J. Schroers: Noble metal high entropy alloys. *Scr. Mater.* **126**, 29 (2017).
65. B. Fultz, L. Anthony, J.L. Robertson, R.M. Nicklow, S. Spooner, and M. Mostoller: Phonon modes and vibrational entropy of mixing in Fe–Cr. *Phys. Rev. B* **52**, 3280 (1995).
66. B. Fultz: Vibrational thermodynamics of materials. *Prog. Mater. Sci.* **55**, 247 (2010).
67. J.A. Munoz, M.S. Lucas, O. Delaire, M.L. Winterrose, L. Mauger, C.W. Li, A.O. Sheets, M.B. Stone, D.L. Abernathy, Y. Xiao, P. Chow, and B. Fultz: Positive vibrational entropy of chemical ordering in FeV. *Phys. Rev. Lett.* **107**, 115501 (2011).

Supplementary Material

To view supplementary material for this article, please visit https://doi.org/10.1557/jmr.2017.366.

https://doi.org/10.1557/jmr.2017.366 Published online by Cambridge University Press